Appendix data: Growth dynamics of vaterite in relation to the physico-chemical properties of its precursor, amorphous calcium carbonate, in the Ca–CO₃–PO₄ system

Yuki Sugiura, Kazuo Onuma and Atsushi Yamazaki

Experimental Method

Measurement of vaterite spherulite growth rate and estimation of surface free energy using direct Ca and CO₃ containing solution mixing and observation cell.

The cell was placed on the stage of a transmitted light optical microscope (BX-60, Olympus Co., Tokyo, Japan), using a white-light lamp as a light source. Photographs of vaterite spherulites were taken during a period of 20–60 s, depending on the supersaturation and PO_4 concentration. We measured the sizes of spherulites in three directions: the longest dimension and at tilts of ± 60° because vaterite spherulites often became distorted forms during growth process. The average of the three lengths was defined as the size of the vaterite spherulite. We measured the size evolution of at least 50 spherulites for each solution condition. The time evolution of spherulite size was fitted using linear approximation and the growth rate (nm/s), R of each condition was

estimated.

The supersaturation of the solution, σ, is defined as

$$\sigma = (C - C_e)/C_e = (I_p/K_{sp})^{1/n} - 1 \qquad (1)$$

where C is the actual concentration, C_e is the equilibrium concentration, I_p is the product

of the ionic activity of $CaCO_3$, K_{sp} is solubility product of the corresponding vaterite

polytypes, and n is the number of ions in the chemical formula ($n = 2$ in this study).

Each solubility of vaterite and pseudo-vaterite were estimated from the Ca ion

concentrations of the corresponding equilibrium solutions using vaterite and

pseudo-vaterite standard (see Resulting section, the details of pseudo-vaterite was

described in Ref (Sugiura et al. 2014)), which were measured by using inductively

coupled-plasma atomic emission spectroscopy (ICP-AES, SI7000, Seiko Instruments

Co., Japan) after filtration of solutions using double filtered method; a 0.22-μm pore

membrane filter and a 0.1 μm centrifuge filter for complete removal of solid particles.

The ionic activities of vaterite and pseudo-vaterite were given using Ca^{2+} and

CO_3^{2-} concentrations in the prepared solutions as

$$I_{p(vaterite,\ pseudo\text{-}vaterite)} = [Ca^{2+}][CO_3^{2-}] \qquad (2)$$

The supersaturation ranges, σ in this study are 0.25–2.13 for vaterite and 0.16–1.89

for pseudo-vaterite. (see Resulting section)

For vaterite and pseudo-vaterite, the relationship between the growth rate R and σ was fitted using the multiple two-dimensional nucleation model (Bennema, 1967a, b; Ookawa, 1977; Saito, 2002). R is expressed using σ as

$$R = K\sigma^{2/3}(1 + \sigma)^{1/3}\{ln(1 + \sigma)\}^{1/6}exp[-\pi\gamma^2/\{3k_B{}^2T^2ln(1 + \sigma)\}] \qquad (3)$$

where K is a experimental constant, k_B is the Boltzmann constant, and T is the absolute temperature.

Eq. 5 is transformed using $1/ln(1 + \sigma)$ as

$$ln[R/[\sigma^{2/3}(1 + \sigma)^{1/3}\{ln(1 + \sigma)\}^{1/6}]] = lnK - \{\pi\gamma^2/(3k_B{}^2T^2)\} \times 1/ln(1 + \sigma) \qquad (4)$$

where γ is the edge free energy of a two-dimensional island, and is calculated using the slope of the plot for $ln[R/[\sigma^{2/3}(1 + \sigma)^{1/3}\{ln(1 + \sigma)\}^{1/6}]]$ against $1/ln(1 + \sigma)$. The slope of plot was often showed as bi-modal trend. We chose steeply-pitched part because it indicated as homogeneous nucleation on the surface of crystals.

The surface free energy of vaterite or pseudo-vaterite, ΔG (mJ/m^2), is expressed as

$$\Delta G = \gamma/(hV)^{1/2} \qquad (5)$$

where h is the step height, and V is the unit cell volume. Vaterite has a spherulitic morphology; thus, it is difficult to observe its surface directly and estimate the step height. In this study, we applied the structural model proposed by LeBail et al. (2011),

in which h is assumed to be a half of the c unit cell parameter, 0.21 nm.

Characterization of vaterite and pseudo-vaterite.

Vaterite spherulites were precipitated in the same manner (1.80 for vaterite and 1.58 for pseudo-vaterite (PO_4-free condition)) as described in the growth rate measurement experiments through optical measurement. The spherulites precipitated on the glass slide were removed from the surface of the glass and collected. The spherulite residues were washed several times using 99.5 % ethanol to stop further reaction and were dried at room temperature.

The C/Ca ratios in each part of the vaterite spherulites that precipitated under various solution conditions were measured using energy dispersive X-ray spectroscopy combined with field emission scanning microscopy (FE-SEM/EDX: FE-SEM, FEI40, FEI Co., the Netherlands EDX, EDAX Genesis, EDAX Japan Co., Japan) using CaF_2-$CaCO_3$-Na_2CO_3 mixture as C/Ca ratio standards. The acceleration voltage and current for the FE-SEM/EDX measurements were 3 kV for SEM observation, 15 kV for EDX analysis, and 140 μA for both.

The crystallite sizes of the precipitates were measured using small-angle X-ray scattering (SAXS: RINT TTR-III, Rigaku Co., Tokyo, Japan). The samples were wrapped with polypropylene films and mounted in transmission measurement cells for

the SAXS measurement. The voltage and current for SAXS measurement were 40 kV

and 100 mA, respectively, using a Cu target to characterize the materials. We used a

Debye-Scherrer optical system. The measured 2θ step was 0.01°; we varied 2θ from

0.06° to 3°, and the time per step was 0.75 s. The data were analyzed using NanoSolver

software (NanoSolver, 3.2, Rigaku Co., Japan), which calculated the crystallite size of

the samples.

The ^{13}C and ^{31}P chemical shifts in vaterite polytypes were measured using a

solid state nuclear magnetic resonance spectrometer (Solid State NMR: JNM-ECX400

JEOL Co., Japan) with a resonance frequency of 400.0 MHz. For all solid state NMR

measurements, magic-angle spinning (MAS) with a single pulse mode for ^{31}P and [13]C

was applied at frequencies of 10000 rpm in 5-mm zirconia rotors. The sample weight

was approximately 1 g, the contact time for ^{31}P MAS measurement was 36 ms with

relaxation delays of 60 s in each interval. The number of repetitions per measurement

was 1400. For ^{13}C MAS measurements, the contact time was 4 ms with relaxation

delays of 15 s in each interval. The number of repetitions per measurement was 500.

The chemical shifts of ^{13}C and ^{31}P were calibrated as 0.0 ppm using hexamethyl

benzene $(CH_3)_6C_6$ and 0.5 M K_2HPO_4–KH_2PO_4 solution with a pH of 8.6.

Characterization for vaterite and pseudo-vaterite.

Fig. 4a shows solid state NMR ^{31}P MAS spectra for rounded vaterite and hollow vaterite. We assumed that the origin of the ^{31}P spectra was the PO_4 species in the samples. The NMR spectrum of hollow vaterite shows a bi modal distribution with peaks at 3.6 ppm and −0.1 ppm. In contrast, the spectrum for rounded vaterite showed a broad unimodal distribution with a peak from 3.1 ppm to 3.7 ppm.

Fig. 4b shows ^{13}C MAS spectra for rounded vaterite and hollow vaterite. Both samples show a broad unimodal peak centered at 169.5 ppm. This peak corresponds to the vaterite CO_3^{2-} chemical shift (169.07 ppm and 170.12 ppm) (Nebel et al., 2008). The two chemical shifts reported by Nebel et al. (2008) were overlapping and detected as a single broad peak in our samples. No difference in peak shift in the spectra was observed between rounded vaterite and hollow vaterite.

The chemical shifts observed in the ^{31}P spectrum for hollow vaterite nearly corresponded to *P1* site (PO_4^{3-}) of octacalcium phosphate (3.6 ppm) and monetite ($CaHPO_4$) PO_4 site (–0.1 ppm) (Hinedi et al., 1992; Bak et al., 2000; Tseng et al., 2004; Tsai and Chan, 2011). These calcium phosphates have been reported as layered structures containing Ca atoms that are essentially similar to the vaterite structure. Vaterite has a layer structure in which six Ca atoms are bonded as rings. CO_3 ions are located in the interspaces between Ca layers and easily migrate from the structure

(Demichelis et al., 2013). Our data suggested that PO_4 partly intercalated instead of CO_3 in the vaterite crystal structure (Figs. 4c and d).

The behavior of chemical shifts observed in the ^{31}P spectrum for rounded vaterite, on the other hand, was similar to that of incorporation behavior in calcite (deKanel and Morse, 1978; Hinedi et al., 1992; Tseng et al., 2004; Gertman et al., 2008). This suggests that PO_4 was absorbed onto the vaterite surface in rounded vaterite (Fig. 4e).

The growth behavior, SAXS analysis and solid state NMR data suggested that the rounded spherulites appeared in the initial stage of growth were pseudo-vaterite with a higher growth rate, and the irregularly shaped that appeared in the late stage of growth were vaterite with a lower growth rate. Furthermore, the PO_4 response behavior was clearly different. The discussion below is based on this model.

Characterization of ACC structure and dynamics.

Raman spectroscopy measurements.

We prepared PO_4-containing ACC by mixing 20 mL of 12.5 mM $CaCl_2$ with $NaHCO_3$ or Na_2CO_3 containing 0–50 μM K_2HPO_4 immediately in Pyrex® glass bottles, which were stirred using a vortex mixer for several seconds (approximately 20 s to 1 min). The pH of the $CaCl_2$ $NaHCO_3$ K_2HPO_4 solution was about 8.6, whereas that of the $CaCl_2$ Na_2CO_3 solution was about 12.0. The ionic strength was adjusted using 1 M

NaCl, 0.1 [M/L]^2, for both types of solutions.

After stirring, ACC-containing solutions were diluted with 20 times volume of chilled (approximately~ −60°C) 99.5% ethanol and stirred at 1000 rpm for several seconds to stop further reaction. The mixed solutions were rapidly centrifuged, washed using chilled (approximately −60°C) 99.5% ethanol several times, and freeze-dried under vacuum at −80°C.

The samples were mounted on glass slides. Raman spectra were obtained using microscopic reflection-type Raman spectroscopy (Renishaw InVia, Micro Raman spectrometer, Renishaw Japan Co., Tokyo, Japan) with a semiconductor laser source with λ_w = 532 nm. All spectra were accumulated in static mode, which gives a wave number resolution of ~0.5 cm^{-1}. The spectrometer was calibrated using Si spectral lines (520.5 cm^{-1}) as a standard. Measurements were conducted in the range of wavenumber 70–3200 cm^{-1}. The time required to measure each spectrum was about 120 s.

Result and Discussions

Measurement of vaterite spherulite growth rate and estimation of surface free energy using direct Ca and CO$_3$ containing solution mixing and observation cell.

The adhesive growth model was obviously inadequate because of its linear

relationship between R and σ. We estimated the growth parameters when the spiral

growth model was applied to the growth rate data.

We calculated the step kinetic coefficient β (Chernov, 1974; Chernov and

Rashkovich, 1987). The β values was strongly influenced the sizes of growth unit. For

example, β value showed 0.4×10^{-4} cm/s in HAP which considered nm size cluster

(Posner's Cluster) was considered as growth unit (Posner and Betts 1975; Onuma and

Ito 1998; Onuma et al. 2000). R of spiral growth model is given as $R = vp$ where v is the

step velocity and p is the slope of the growth hillock. The v and p were explained using

σ, β and equilibrium concentration. R is expressed as

$$R = hCe\beta Zk_BT\sigma ln(1 + \sigma)/19\gamma a \tag{13}$$

The a is the radius of growth unit that is considered to be 1 nm (Gebauer et al.

2010; Demichelis et al., 2011). β/γ value was estimated using the slope in the plot for

$19aR$ against $hC_ek_BT\sigma ln(1 + \sigma)$. The equilibrium concentration, C_e was 6.14×10^{22} m^{-3}

for vaterite and 7.22×10^{22} m^{-3} for pseudo-vaterite. When we applied the γ value

estimated from the two-dimensional nucleation model to the calculated β/γ, β was 1.65

cm/s for vaterite and 4.13 cm/s for pseudo-vaterite, respectively.

These values of β are approximately three orders of magnitude larger than

those of proteins or hydroxyapatite (Onuma et al., 1996; Sazaki et al., 1996) and are

comparable to those of soluble inorganic crystals (Malkin et al., 1989). When we use the cluster-based growth for vaterite (see the discussion part for details), as was confirmed in previous studies, the application of the spiral growth model to the growth rate data was inadequate.

Dynamics and structures of ACC particles in Ca–CO$_3$–PO$_4$ system

Raman spectroscopic analysis of structure of ACC structure with PO$_4$ concentration

Figs. 8a–d show the Raman spectra of ACC aggregates in PO$_4$ solutions and the reference spectrum of amorphous calcium phosphate (ACP). The strongest peaks of ACC samples were all observed at about 1085 cm^{-1}, which could be attributed to Ca–CO$_3$ bands corresponding to the symmetric stretching of calcite (1085 cm^{-1}) or vaterite (1089 cm^{-1}) (Figs. 8a and b) according to previous studies (Kontoyannis and Vagenas, 2000; Gopi et al., 2013). Unfortunately, the strongest peaks corresponding to the symmetric stretching of non-hydrated calcium carbonate phases are at about 1085 cm^{-1} (1085 cm^{-1} for calcite,   1089 cm^{-1} for vaterite, and 1087 cm^{-1} for aragonite); thus, this peak cannot be used for the analysis of ACC structure.

With the increase in PO$_4$ concentration, a peak at approximately 1075 cm^{-1} corresponding to an extra symmetric stretching vibration mode of vaterite was observed.

A slight peak shift was observed with an increase in PO_4 concentration, and the peak intensity increased with increasing PO_4. For example, the peak had a relative intensity of about 10 without any peak-split in the PO_4-free solution; however, it changed to bi modal peaks in the 50 μM PO_4 solutions with a relative intensity of about 60. This indicates that Ca–CO_3 chemical bonds similar to those observed in the ration of vaterite structure increased with increasing PO_4 concentration. In addition to symmetry-stretching vibration, Raman vibrations corresponding to lattice mode and plane bending were observed in the vaterite structure with an increase in PO_4 concentration. The intensities corresponding to the Raman bands for vaterite (around 118 cm^{-1} and 301 cm^{-1} in the lattice mode, 740.4 cm^{-1} and 751.1 cm^{-1} in the plane bending mode, respectively) increased with the PO_4 concentration (Figs. 8c and d).

The peak corresponding to the Raman band, 301 cm^{-1}, shifted toward higher wavenumber with the PO_4 concentration such that the 301.2 cm^{-1} peak in the PO_4-free solution shifted to 306.5 cm^{-1} in the 50 μM PO_4-containing solution. The peak at 118 cm^{-1}, on the other hand, shifted toward a lower wavenumber with increasing PO_4 concentration such that the 118.4 cm^{-1} peak in the PO_4-free solution shifted to 111.8 cm^{-1} in a 50 μM PO_4-containing solution (Fig. 8c).

In contrast to the peak shift observed in the lattice mode, a slight shift was

observed in the plane bending mode of Raman bands (740.4 cm^{-1} and 751.1 cm^{-1}) with changes in the PO_4 concentration (Fig. 8d).

An extra broad peak appeared at approximately 210 cm^{-1} with an increase in the PO_4 concentration, which corresponds to the lattice mode of aragonite, although aragonite was not observed in the precipitates.

Large shifts in the Raman bands corresponding to symmetric stretching and lattice modes of the vaterite structure were observed and a slight shift of the plane bending mode was observed. A summary of the shift in Raman bands is shown in Table 2. The asymmetric stretching bands corresponding to the vaterite structure were too weak to be detected.

Evidence of attributed bands for Ca–PO_4 in ACC samples was not detected under these solution conditions.
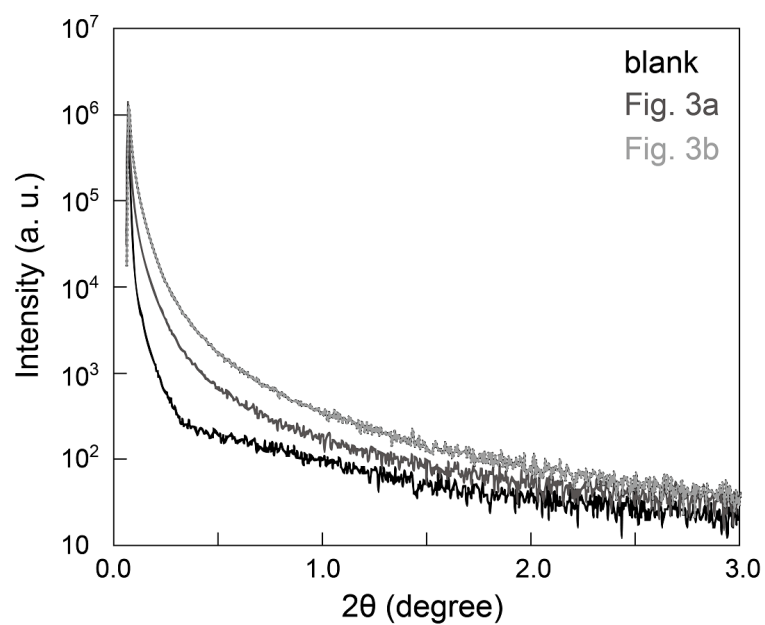
Fig. S1. XRD pattern corresponding to blank, Fig. 3a (irregular shape of vaterite spherulites) and Fig.
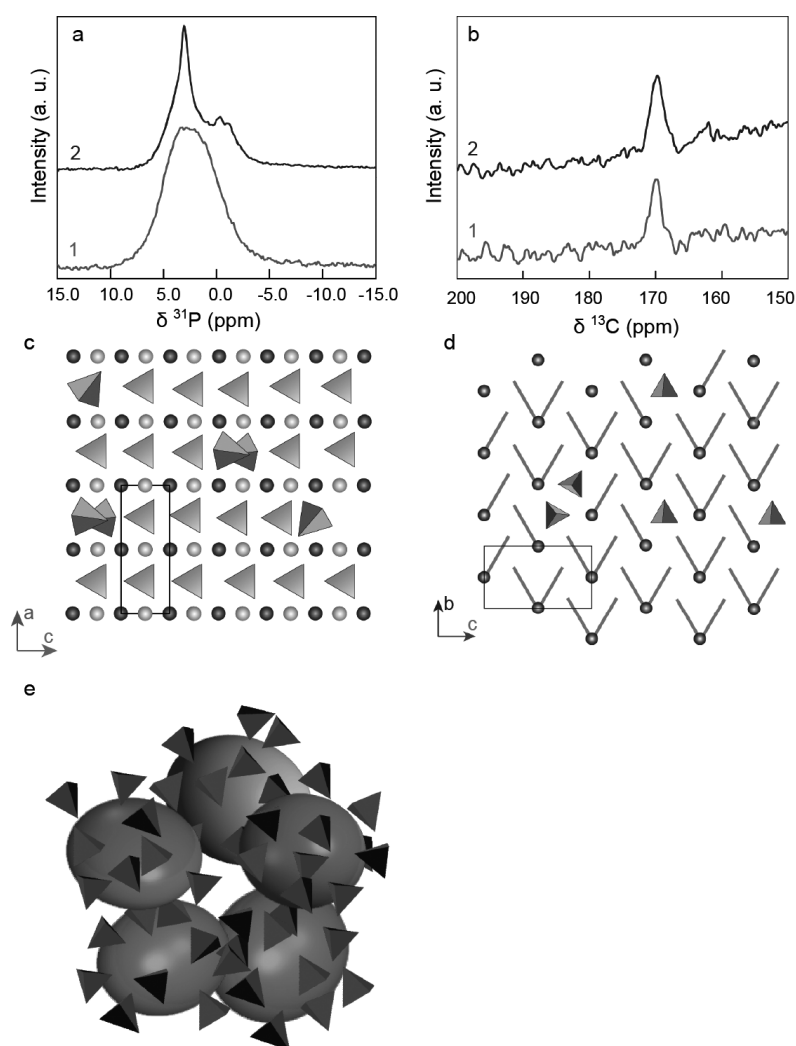
3b (hollow structure of vaterite) for SAXS measurements.

Fig. S2. ^{31}P MAS and ^{13}C MAS NMR spectra of rounded vaterite and hollow vaterite, and schematic images of vaterite and pseudo-vaterite in relation to incorporated PO_4. (**a**) ^{31}P solid state MAS NMR spectra. 1: rounded whole spherulite. 2: hollow spherulite. (**b**) ^{13}C solid state MAS NMR spectra. 1: rounded whole spherulite. 2: hollow spherulite. (**c**) Schematic image of incorporation PO_4 into the vaterite crystal structure viewed from the *b*-axis. PO_4 (triangular pyramids) has replaced CO_3 (triangles) in the spaces between the Ca layers (Ca atoms are indicated as light grey (near side) and black (back side) spheres). (**d**) Schematic image of incorporation of PO_4 into the vaterite structure viewed from the *a*-axis. Grey rods correspond to CO_3. The open black square of (**c**) and (**d**) denote a unit cell in the vaterite crystal structure. (**e**) Schematic image for adsorption of PO_4 onto pseudo-vaterite. Spheres indicate pseudo-vaterite crystallites, and triangular pyramids indicate PO_4 adsorbed onto the surface of the pseudo-vaterite crystallite.
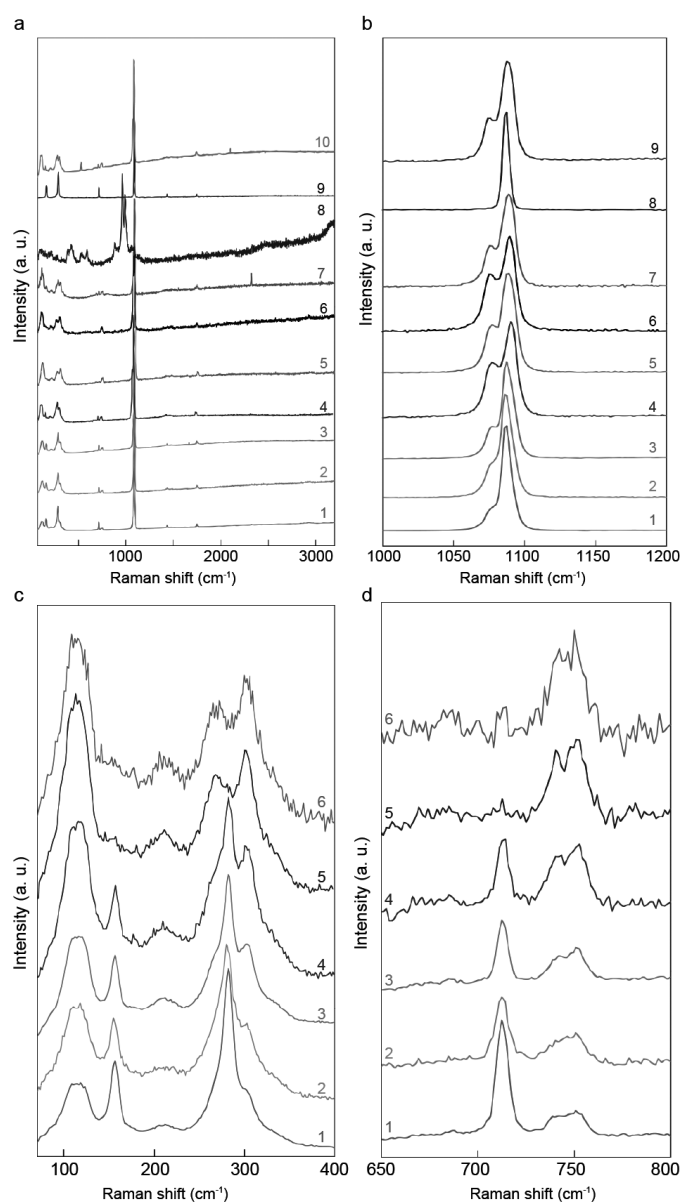
Fig. S3. (**a**) Raman spectra of ACC at 70–3200 cm^{-1} precipitated in solutions containing no PO$_4$ (1), 5 μM PO$_4$ (2), 10 μM PO$_4$ (3), 15 μM PO$_4$ (4), 20 μM PO$_4$ (5) and 50 μM PO$_4$ (6). The spectrum of ACC precipitated in Na$_2$CO$_3$-CaCl$_2$ solution is (7) and that of ACP precipitated in K$_2$HPO$_4$–CaCl$_2$ solution is (8). Spectrum of vaterite is (9) and that of calcite is (10). (**b**) Expanded Raman spectra at 1000–1200 cm^{-1} for the same samples as in (A). PO$_4$-free (1), 5 μM PO$_4$ (2), 10 μM PO$_4$ (3), 15 μM PO$_4$ (4), 20 μM PO$_4$ (5), 50 μM PO$_4$ (6), Na$_2$CO$_3$–CaCl$_2$ ACC (7), calcite (8), vaterite (9). A bi modal trend was observed with increasing PO$_4$ concentration. (**c**) Expanded Raman spectra at 70–400 cm^{-1} for the same samples as (1) to (6) in (**a**). (**d**) Expanded Raman spectra at 650–800 cm^{-1} for the same samples as (1) to (6) in (**a**).

References Cites

Bennema P. (1967a) Analysis of crystal growth models for slightly supersaturated solutions. Journal of Crystal Growth, 1, 278-286.

Bennema P. (1967b) Interpretation of the relation between the rate of crystal growth from solution and the relative supersaturation at low supersaturation. Journal of Crystal Growth, 1, 287-292.

Chernov A. A. (1974) Stability of faceted shapes. Journal of Crystal Growth, 24/25, 11-31.

Chernov A. A. and Rashkovich L. N. (1987) Spiral crystal growth with nonlinear dependence of step growth rate on supersaturation: the {110} faces of KH_2PO_4 crystals in aqueous solution. Journal of Crystal Growth, 84, 389-393.

de Kanel J. and Morse J. W. (1978) The chemistry of orthophosphate uptake from seawater on to calcite and aragonite. Geochimica et Cosmochimica Acta, 42, 1335-1340.

Gertman R., Shir I. B., Kababya S. and Schmidt A. (2008) *In situ* observation of the internal structure and composition of biomineralized *Emiliania huxleyi* calcite by solid state NMR spectroscopy. Journal of American Chemical Society, 130, 13425-13432.

Gopi S., Subramanian V. K. and Palanisamy K. (2013) Aragonite-calcite-vaterite: A temperature influenced sequential polymorphic transformation of $CaCO_3$ in the presence of DTPA. Material Research Bulletin, 48, 1906-1912.

Hinedi Z. R., Goldberg S., Chang A. C. and Yesinowski J. P. (1992) A ^{31}P and ^{1}H MAS NMR study of phosphate sorption onto calcium carbonate. Journal of Colloidal Interface Science, 152, 141-160.

Kontoyannis C. G. and Vagenas N. V. (2000) Calcium carbonate phase analysis using XRD and FT-Raman spectroscopy. The Analyst, 125, 251-255.

LeBail A., Ouhenia S. and Chateigner D. (2011) Microtwinning hypothesis for a more ordered vaterite model. Powder Diffractions, 26, 16-21.

Nebel H., Neumann M., Mayer C. and Epple M. (2008) On the structure of amorphous calcium carbonate–A detailed study by solid-state NMR spectroscopy. Inorganic Chemistry, 47, 7874-7879.

Ookawa A. (1977) Chapter 1: Growth of complete crystal. Crystal growth. Syokabo Co., Japan. pp.2-28. (in Japanese)

Tsai T. W. T. and Chan J. C. C. (2011) Recent progress in the solid-state NMR studies of biomineralization. Annual Report of NMR Spectroscopy, 73, 1-61.

Tseng Y. H., Zhan J., Lin K. S. K., Mou C. Y. and Chan J. C. C. (2004) High

resolution ^{31}P NMR study of octacalcium phosphate. Solid State Nuclear Magnetic

Resonance, 26, 99-104.